The FASEB Journal

FASEB
Federation of American Societies for Experimental Biology

RESEARCH ARTICLE

Human Amniotic Fluid-Derived Exosomes Alleviate Neuropathic Pain by Inducing an Anti-Inflammatory Transition in Microglia

Qian Li[1,2] | Hang Dai[3] | Sha Zhang[1,2] | Ping Li[2,4] | Lin Peng[1] | Yulu Chen[1] | Qulian Guo[1,2] | Yong Yang[1,2]

[1]Department of Anesthesiology, Xiangya Hospital, Central South University, Changsha, China | [2]National Clinical Research Center for Geriatric Disorders, Xiangya Hospital, Central South University, Changsha, China | [3]Department of Anesthesiology, Guangdong Second Provincial General Hospital, Guangzhou, China | [4]Department of Obstetrics, Xiangya Hospital, Central South University, Changsha, China

Correspondence: Yong Yang (yangwulf@163.com)

Received: 4 February 2025 | **Revised:** 29 April 2025 | **Accepted:** 14 May 2025

Funding: This work was supported by the Natural Science Foundation of Hunan Province (Grant 2022JJ30975).

Keywords: amniotic fluid | anti-inflammatory | exosome | microglia | neuropathic pain

ABSTRACT

Neuropathic pain is a chronic and debilitating condition characterized by persistent discomfort. Modulation of microglial homeostasis and associated neuroinflammation plays a pivotal role in the pathogenesis of neuropathic pain. Microglia exhibit diverse and dynamic states that contribute to the expression of various cytokines and mediators involved in inflammation. Based on the well-documented anti-inflammatory and neuroprotective properties of human amniotic fluid-derived exosomes (AF-Exos), we tested the hypothesis that AF-Exos could alleviate neuropathic pain by modulating the microglial homeostasis both in vivo and in vitro. Spared nerve injury (SNI) surgery was performed on Kunming mice to induce neuropathic pain. AF-Exos, utilized for both in vivo and in vitro interventions, were isolated from pregnant women in their second or third trimesters. The fluorescein-labeled AF-Exos were detected in both the ipsilateral dorsal horn of the spinal cord and lipopolysaccharide (LPS)-induced BV2 cells. Intrathecal administration of AF-Exos alleviated mechanical allodynia in the ipsilateral hind paw of SNI mice. Following nerve injury, AF-Exos suppressed the expression of IL-1β, IL-6, and nitric oxide in microglia, while upregulating the expression of IL-10. Moreover, AF-Exos promoted a reduction in the $CD86^{+}/CD206^{+}$ ratio of BV2 cells and upregulated Arg-1 expression, leading to a transition in the functional state of LPS-induced BV2 cells. Notably, the effects of second-trimester AF-Exos were superior to those of third-trimester AF-Exos. The analgesic effects of human AF-Exos on neuropathic pain may be attributed to their ability to suppress neuroinflammation by promoting the transition of microglia to an anti-inflammatory phenotype.

Abbreviations: AF-Exos, amniotic fluid-derived exosomes; AFSCs, amniotic fluid stem cells; ANOVA, analysis of variance; Arg-1, arginase 1; CD, cluster of differentiation; cDNA, complementary DNA; CT, cycle threshold; DAPI, 4′,6-diamidino-2-phenylindole; EVs, extracellular vesicles; GAPDH, glyceraldehyde-3-phosphate dehydrogenase; HSPD1, heat shock protein family D member 1; HSPG2, heparan sulfate proteoglycan 2; IL, interleukin; LPS, lipopolysaccharide; NO, nitric oxide; PBS, phosphate-buffered saline; PWMT, paw withdrawal mechanical threshold; qPCR, quantitative polymerase chain reaction; RQ, relative quantification; SD, standard deviation; SNI, spared nerve injury; THBS1, thrombospondin 1; TSG101, tumor susceptibility gene 101.

Qian Li and Hang Dai should be considered joint first authors.

1 | Introduction

The estimated global prevalence of neuropathic pain is approximately 10% of the general population [1]. Current treatments for neuropathic pain frequently exhibit limited efficacy and are associated with undesirable adverse effects [2, 3], and further studies are required to explore effective therapies for patients with neuropathic pain.

Microglia, the professional macrophages of the central nervous system, contribute to the development of pain hypersensitivity upon stimulation, a characteristic feature of neuropathic pain [4, 5]. Peripheral nerve injuries trigger reactive changes in microglia, characterized by cell proliferation and morphological remodeling. These dynamic state transitions play a pivotal role in the development of neuropathic pain [6, 7]. In the central nervous system, microglia exhibit a dynamic and plastic continuum of functional states. Following neural injury, their functional states undergo multidimensional transformations, which are determined by local microenvironmental signals and disease-specific contexts [8]. Among these, the Cluster of Differentiation (CD) 86-enriched phenotype may promote inflammatory responses, while the CD206-enriched phenotype may contribute to tissue repair [9, 10]. The imbalance in these functional states participates in the pathogenesis of neuropathic pain by modulating neuroinflammatory processes.

Perinatally derived tissues and cells exhibit analgesic effects. Human umbilical cord mesenchymal stem cells may alleviate mechanical hyperalgesia and thermal allodynia in neuropathic pain [11]. Amniotic fluid contains several key proteins, including Heat Shock protein family D member 1 (HSPD1), heparan sulfate proteoglycan 2 (HSPG2), and thrombospondin 1 (THBS1) [12]. Notably, HSPD1, HSPG2, and THBS1 exhibit immunosuppressive functions through diverse and distinct molecular mechanisms [13–15]. Moreover, cell-free amniotic fluid, composed of soluble components and extracellular vesicles (EVs), contains proteins whose concentrations fluctuate as pregnancy progresses [16], and exhibits immunomodulatory, anti-inflammatory, and neuroprotective functions [17–19]. Exosomes, a subset of EVs, are released via endosome-dependent pathways, and they transport nucleic acids, proteins, lipids, cytokines, and metabolites [20]. Human amniotic fluid-derived exosomes (AF-Exos) can be directly isolated from the amniotic fluid and safely administered systemically at doses consistent with a clinically compliant formulation, rendering them a valuable diagnostic and therapeutic tool [21]. Therefore, we hypothesized that AF-Exos hold significant potential for the treatment of neuropathic pain.

In the present study, we investigated the analgesic effects of AF-Exos derived from pregnant women in different trimesters on neuropathic pain in a spared nerve injury (SNI) mouse model, as well as their impact on neuroinflammation. Additionally, we examined the effects of AF-Exos on microglial homeostasis transition in lipopolysaccharide (LPS)-induced BV2 cells to elucidate the underlying analgesic mechanisms. Our study provides comprehensive evidence that AF-Exos can effectively alleviate neuropathic pain by modulating microglial homeostasis and neuroinflammation, thereby offering a novel therapeutic strategy for managing neuropathic pain.

2 | Materials and Methods

2.1 | Isolation of AF-Exos

The study was approved by the Medical Ethics Committee of Xiangya Hospital, Central South University, China (approval number 202104175). The trial was registered before patient enrollment at the Chinese Clinical Trial Registry (ChiCTR2100051218, principal investigator: Yong Yang, date of registration: September 16, 2021). Participants provided written informed consent. Pregnant women aged 28–35 years without pregnancy-related complications were recruited, whereas those with inflammatory or infectious diseases were excluded. Second-trimester amniotic fluid was collected through amniocentesis from five pregnant women at 13–27 weeks of gestation. Third-trimester amniotic fluid was collected from five pregnant women at 28–38 weeks of gestation during cesarean delivery. AF-Exos were isolated using a commercially available total exosome isolation kit (Thermo Fisher Scientific, Waltham, MA, USA, Cat#4484453) following the manufacturer's instructions. Briefly, the amniotic fluid was centrifuged at 2000×*g* at 4°C for 30 min. Subsequently, the supernatant was centrifuged at 10000×*g* at 4°C for 30 min. Finally, the supernatant was treated with the total exosome isolation solution and incubated at room temperature for 30 min. Thereafter, the incubation solution was centrifuged at 10000×*g* at 4°C for 60 min, and the precipitate was air-dried. The final exosome pellet was resuspended in phosphate-buffered saline (PBS) and stored at −80°C.

2.2 | AF-Exos Characterization

The protein concentration of the exosome solution was determined using the Bicinchoninic Acid Assay (CWBIO, Beijing, China, Cat#CW0014S). Samples were fixed with 1% glutaraldehyde and stained with 1% phosphotungstic acid. Subsequently, the exosomes were observed using a transmission electron microscope (Thermo Fisher Scientific) at a voltage of 80 kV. The samples were diluted in the ratio of 1:100 with PBS and subjected to nanoparticle tracking analysis (Particle Metrix, Innsbruck, Germany) for particle size testing. The classical exosomal markers, including CD9, CD63, tumor susceptibility gene 101 (TSG101), and Calnexin, were detected by western blot.

2.3 | Animals

The animal study was approved by the Animal Ethics Committee of Central South University, China (approval number CSU20220204). Animal experiments were conducted in accordance with the ARRIVE 2.0 guidelines and adhere to the principles of the 3Rs. Twenty-four Specific-pathogen-free male Kunming outbred mice (7–8 weeks old, 30–35 g, RRID: MGI: 5651867) were provided by the Hunan SJA Laboratory Animal Co. Ltd. Mice were randomly divided into four groups: sham surgery (Sham); SNI surgery and intrathecal PBS (SNI + PBS); SNI surgery and intrathecal second-trimester AF-Exos (SNI + 2nd AF-Exos); and SNI surgery and intrathecal third-trimester AF-Exos (SNI + 3rd AF-Exos), with six mice in each group ($n = 6$). The mice were housed in a controlled environment with a 12/12-h light/dark cycle with ad libitum

access to food and water. The in vivo experimental procedure is shown in Figure 1A.

2.4 | Establishment of the Neuropathic Model

The SNI model was established using the following protocol. Briefly, the mice were anesthetized with a 50 mg·kg^{-1} dose of 1% pentobarbital sodium. A 1–2-cm longitudinal incision was made on the proximal aspect of the left knee under sterile conditions. The subcutaneous tissues and muscles were bluntly dissected to reach the sciatic nerve. The common peroneal and tibial nerves were tightly ligated using a 5.0 silk suture, and then transected to prevent injury to the sural nerve. In the Sham group, wound exposure was performed without nerve ligation or transection. Mice with postoperative neurological deficits were excluded.

2.5 | Drug Treatment and Behavioral Analysis

Drugs were delivered intrathecally through a direct lumbar puncture between the L5 and L6 spinal levels in awake mice. Mice were restrained appropriately for administering the intrathecal injection. The success of the intrathecal injection was confirmed through a brisk tail-flick test, and mice showing signs of spinal cord injury were excluded. On Days 1, 2, and 3 after surgery, 7 μL PBS or AF-Exos (1 μg/μL) was intrathecally administered using a 30 G needle. The paw withdrawal mechanical threshold (PWMT) was measured using a von Frey filament (Stoelting, Wood Dale, IL, USA). Tests were performed 1 day before surgery and on Days 1, 3, 5, and 7 after surgery by an investigator blinded to the experimental grouping. After adaptation for 30 min in the testing environment, a von Frey filament was applied, bent to reach a 30° angle, and held on the lateral plantar surface of the hind paw for 3 s. Positive reactions were indicated by foot licking or withdrawal. The procedure was repeated five times to obtain average data.

2.6 | Cell Culture and Treatment

BV2 murine microglial cell line was obtained from National Collection of Authenticated Cell Cultures (Cat#SCSP-5208, RRID: CVCL_0182). The cells were cultured in Dulbecco's modified Eagle's medium (Gibco, Gaithersburg, MD, USA, Cat#11965092) supplemented with 10% fetal bovine serum (Gibco, Cat#10099141). The cells were maintained in an incubator at 37°C with 5% CO_2. The cells were randomly divided into four groups as follows: no treatment (Control) group; group treated with 250 ng/mL LPS (Sigma-Aldrich, St. Louis, MO, USA, Cat#L2630-10MG) (LPS + PBS); group treated with 250 ng/mL LPS and 200 μg/mL second-trimester AF-Exos (LPS + 2nd AF-Exos); and group treated with 250 ng/mL LPS and 200 μg/mL third-trimester AF-Exos (LPS + 3rd AF-Exos). The in vitro experimental procedure is presented in Figure 1B.

2.7 | Detection of AF-Exos Uptake Using Fluorescence Microscopy

AF-Exos were stained with PKH26 using the PKH26 Red Fluorescent Cell Linker Kit (Sigma-Aldrich, Cat#MINI26). The nuclei were stained using 4′,6-diamidino-2-phenylindole (DAPI) Fluoromount-G (SouthernBiotech, Birmingham, AL, USA, Cat#0100-20). The cytoskeleton was stained with Cytoskeletal Staining Reagent (Yisike Biotechnology, Xiangxi, Hunan, China, Cat#Eph-1-100). Following 3 days of treatment with AF-Exos, the lumbar spinal cord was subjected to transcardial perfusion with normal saline, carefully resected, and subsequently frozen at −20°C. The tissues were embedded and sectioned into 10-μm slices using a Cryostat Microtome (Leica, Wetzlar, Germany). Slices were fixed with 4% paraformaldehyde, washed with PBS, and then mounted with DAPI Fluoromount-G. BV2 cells treated with AF-Exos for 24 h were fixed in 4% paraformaldehyde, washed with PBS, subsequently stained with Cytoskeletal Staining Reagent, and finally mounted using DAPI Fluoromount-G. Slices and cells were observed under a fluorescence microscope (Olympus, Tokyo, Japan). The quantitative analysis of exosome uptake in BV2 cells was performed using the EVAnalyzer plugin in FIJI (V1.54p, http://fiji.sc, RRID: SCR_002285) following the methods described previously [22].

2.8 | CCK8 Assay

The treated BV2 cells were incubated with a Cell Counting Kit-8 solution (MedChemExpress, Monmouth Junction, NJ, USA, Cat#HY-K0301) at 37°C for 4 h. Absorbance values were measured at 450 nm using a microplate reader (BioTek, Winooski, VT, USA).

2.9 | Nitric Oxide (NO) Assay

NO levels were measured by detecting the accumulation of sodium nitrite in the BV2 cell culture supernatants using a Griess Reaction Kit (Beyotime, Shanghai, China, Cat#S0021S). The supernatants of treated BV2 cells were incubated with equal volumes of Griess Reagent I and II at room temperature. The absorbance values were measured at 540 nm using a microplate reader (BioTek).

2.10 | Western Blot

The lumbar spinal cord tissues were resected on Day 7 after surgery. Total protein was isolated from exosomes, lumbar spinal cord tissues, and BV2 cells using Radio Immunoprecipitation Assay Lysis Buffer (Beyotime, Cat#P0013B). Protein samples were loaded in equivalent quantities, specifically 20 μg for exosome proteins and 50 μg for spinal cord and BV2 cell proteins. Protein samples were separated using sodium dodecyl sulfate–polyacrylamide gel electrophoresis and transferred onto polyvinylidene fluoride membranes. After blocking with 5% non-fat milk for 2 h at room temperature, the membranes were incubated overnight at 4°C with primary antibodies, including CD9 (1:1000; Abcam, Cat#ab92726, RRID: AB_10561589), CD63 (1:2000; Abcam, Cat#ab134045, RRID: AB_2800495), TSG101 (1:1000; Cell Signaling, Cat#72312, RRID: AB_2927716), and Calnexin (1:1000; Cell Signaling, Cat#2679, RRID: AB_2228381), interleukin (IL)-1β (1:500; Proteintech, Cat#26048-1-AP, RRID: AB_2880351), IL-10 (1:500; Abclonal, Cat#A20723, RRID: AB_3695580), CD16

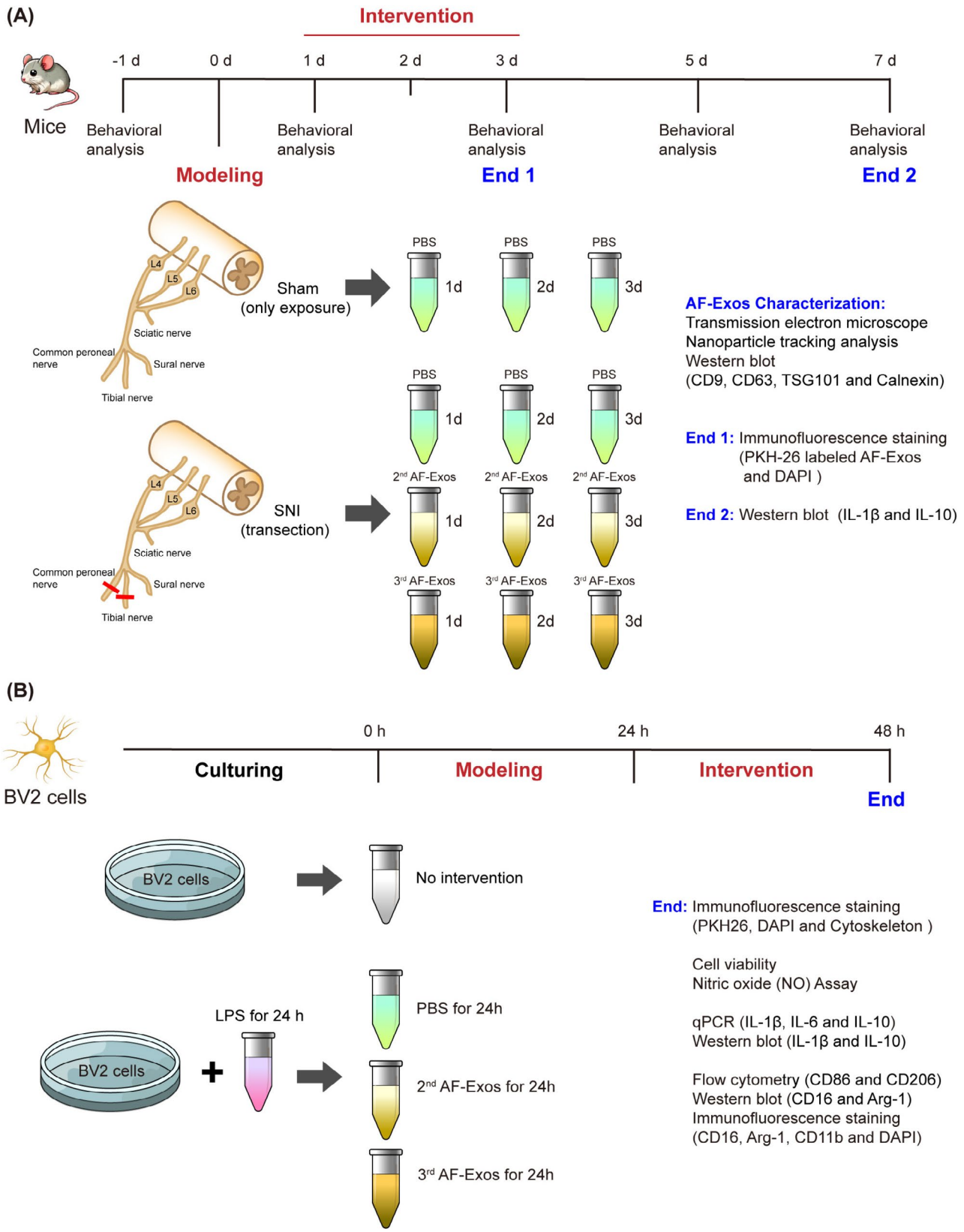

FIGURE 1 | The experimental timelines and procedures. (A) In vivo experiment timeline and procedure. (B) In vitro experiment timeline and procedure. AF-Exos, amniotic fluid-derived exosomes; Arg-1, arginase 1; CD, cluster of differentiation; DAPI, 4′,6-diamidino-2-phenylindole; IL, interleukin; LPS, lipopolysaccharide; PBS, phosphate-buffered saline; qPCR, quantitative polymerase chain reaction; SNI, spared nerve injury; TSG101, tumor susceptibility gene 101.

(1:500; Proteintech, Cat#16559-1-AP, RRID: AB_2878279), arginase 1 (Arg-1) (1:1000; Proteintech, Cat#16001-1-AP, RRID: AB_2289842), β-actin (1:2000; Proteintech, Cat#20536-1-AP, RRID: AB_10700003), and glyceraldehyde-3-phosphate dehydrogenase (GAPDH) (1:2000; Proteintech, Cat#60004-1-Ig, RRID: AB_2107436). Subsequently, they were incubated with secondary antibodies (1:5000; Abiowell, Cat#AWS0001, RRID: AB_3676030 and Cat#AWS0002, RRID: AB_3676029) for 1.5 h at room temperature. The bands were finally visualized with the Omni-ECL ultra-sensitive chemiluminescent detection kit (Yamei Biotech, Shanghai, China, Cat#SQ201L). Quantitative analysis was performed using FIJI software (V1.54p).

2.11 | Quantitative Polymerase Chain Reaction (qPCR)

Total RNA was extracted from BV2 cells using the TransZol Up (TransGen Biotech, Beijing, China, Cat#ET111-01). RNA concentration and purity were assessed using the NanoDrop 2000 Spectrophotometer (Thermo Fisher Scientific). A total of 1 μg RNA was reverse transcribed to complementary DNA (cDNA) using TransScript All-in-One First-Strand cDNA Synthesis SuperMix for qPCR (TransGen Biotech, Cat#AT341-02). qPCR was subsequently performed using PerfectStart Green qPCR SuperMix (TransGen Biotech, Cat#AQ601-01) in a total reaction volume of 20 μL containing 1 μL of 5-fold diluted cDNA product. The probes for IL-1β, IL-6, IL-10, and GAPDH were designed and provided by Nanjing GenScript Biotech Corp. The primer sequences used are listed in Table 1. The cycle threshold (CT) values were normalized to those of GAPDH. Relative quantification (RQ) was calculated using the formula $RQ = 2^{-\Delta\Delta CT}$.

2.12 | Flow Cytometry

BV2 cells were treated with 0.25% trypsin–EDTA solution (Procell Life Technology, Wuhan, China, Cat#PB180225) at 37°C for 1 min. After centrifugation, the cell pellet was washed three times with Flow Cytometry Staining Buffer (Thermo Fisher Scientific, Cat#00-4222-57), and subsequently resuspended in the same buffer. Then the cells were incubated with CD86 (1:400; Thermo Fisher Scientific, Cat#17-0862-81, RRID: AB_469418) and CD206 antibodies (1:100; Thermo Fisher Scientific, Cat#17-2061-80, RRID: AB_2637419) for 30 min in the dark. The cells were then centrifuged at 400×g and resuspended in Flow Cytometry Staining Buffer. The fluorescence intensities of CD86 and CD206 in BV2 cells were detected using flow cytometry (Beckman, Miami, FL, USA).

TABLE 1 | Primer sequences.

Gene	Primer sequence (5′ to 3′)
IL-1β	Forward: ATGAAGGGCTGCTTCCAAAC
	Reverse: TGATGTGCTGCTGCGAGATT
IL-10	Forward: GGACAACATACTGCTAACCGACTC
	Reverse: AAACTGGATCATTTCCGATAAGG
IL-6	Forward: CTTGGGACTGATGCTGGTGA
	Reverse: GGTATAGACAGGTCTGTTGGGAG
GAPDH	Forward: CCCTTAAGAGGGATGCTGCC
	Reverse: TACGGCCAAATCCGTTCACA

2.13 | Immunofluorescence Staining

The treated BV2 cells were fixed with 4% formaldehyde, permeabilized with 0.3% Triton, blocked with 5% bovine serum albumin, and then incubated overnight at 4°C with CD16 (1:300; Proteintech, Cat#16559-1-AP, RRID: AB_2878279), Arg-1 (1:200; Proteintech, Cat#16001-1-AP, RRID: AB_2289842), and CD11b (1:200; Abcam, Cat#ab133357, RRID: AB_2650514) antibodies. The cells were then incubated with a goat anti-rabbit IgG secondary antibody (1:500; Abiowell, Cat#AWS0001, RRID: AB_3676030). Nuclei were stained with DAPI Fluoromount-G. Images were captured using a fluorescence microscope (Olympus). Quantitative analyses of CD11b, CD16, and Arg-1 expression in BV2 cells were performed using FIJI software (V1.54p). For each condition, a total of nine random fields from three independent experiments (3 fields per experiment) were analyzed, with approximately 500–850 cells counted per group. Fluorescence intensities for CD16, Arg-1, and CD11b immunostaining were quantified and normalized to DAPI-positive nuclei count to derive per-cell mean fluorescence intensity values.

2.14 | Statistical Analysis

All data were analyzed using GraphPad Prism (V9.5.0, http://www.graphpad.com/, RRID: SCR_002798). Normally distributed or approximately normally distributed data are presented as mean ± standard deviation (SD). The comparison between the two groups was conducted using an unpaired two-tailed *t*-test. The results of the behavioral tests were analyzed using a two-way analysis of variance (ANOVA) followed by Bonferroni's multiple-comparison test. Biochemical and morphological data were analyzed using a one-way ANOVA followed by Bonferroni's multiple-comparison test. $p < 0.05$ was considered statistically significant. Each in vitro experiment was successfully repeated at least three times. The sample size for each group in the in vivo experiments was based on previously published studies that utilized similar methodologies.

3 | Results

3.1 | Characterization of AF-Exos

Typical teacup-like structures were observed in both second and third-trimester AF-Exos using transmission electron microscope (Figure 2A). The results of nanoparticle tracking analysis indicated that the diameters of exosomes in the second and

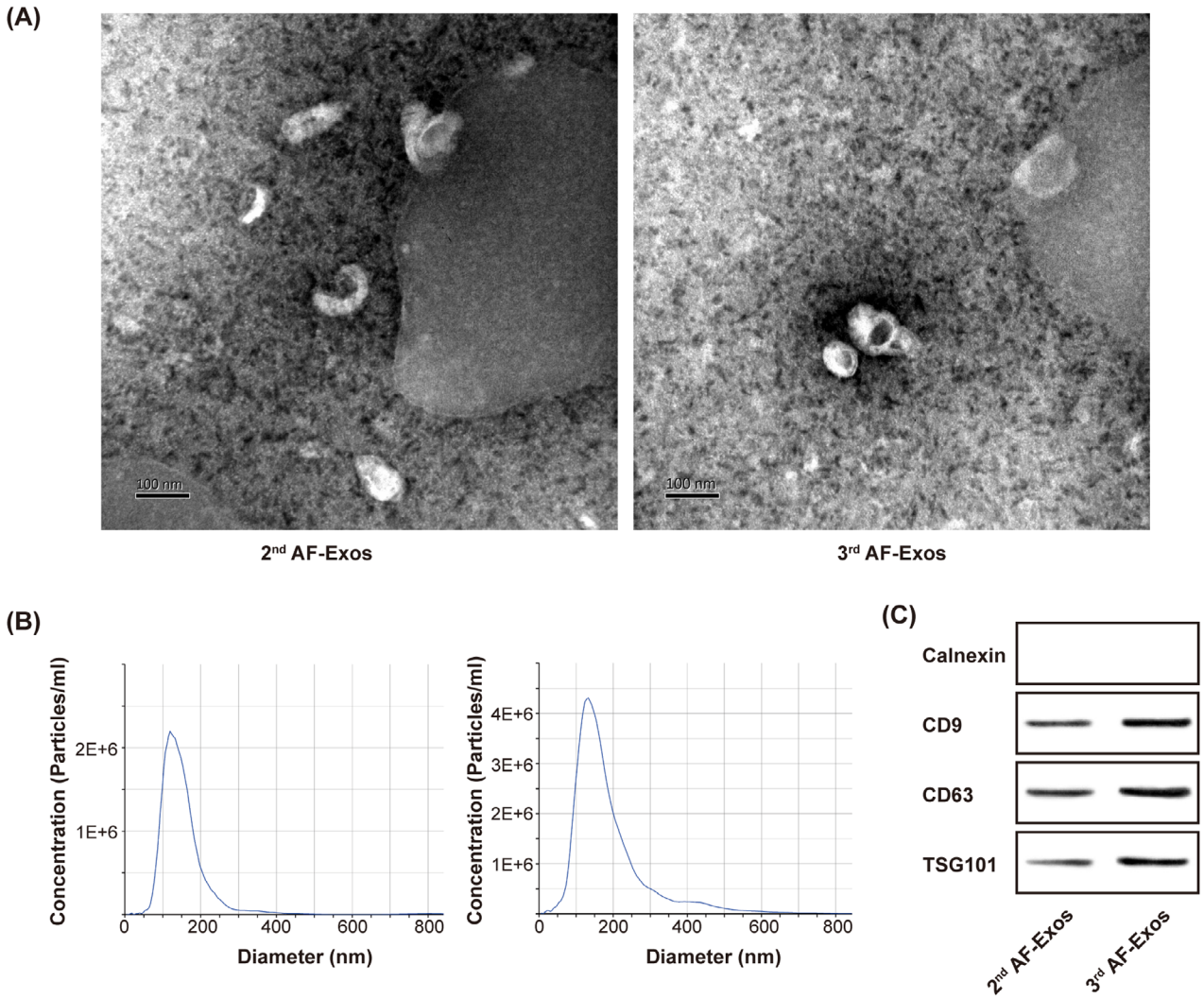

FIGURE 2 | Characterization of human AF-Exos. (A) Transmission electron microscopy showing typical teacup-like structures of AF-Exos. (B) Diameters of AF-Exos in the second and third trimesters. (C) Protein expression levels of exosomal markers.

third trimesters were 134.7 ± 49.4 and 151.1 ± 73.1 nm, respectively (Figure 2B), which were consistent with typical exosomal characteristics [23]. Classical exosomal markers, including CD9, CD63, and TSG101, were expressed positively in AF-Exos, while Calnexin, which is typically absent in exosome preparations, was not detected (Figure 2C), confirming the successful isolation of AF-Exos [24, 25].

3.2 | Uptake of AF-Exos

PKH26, a lipophilic fluorescent dye, marks the exosomal membrane, allowing for the visualization of the endocytosis process of exosomes. Fluorescence microscopy observations revealed detectable PKH26-positive signals in the ipsilateral dorsal horn of the spinal cord in SNI mice (Figure 3A), as well as in LPS-induced BV2 cells (Figure 3B), indicating that exosomes were internalized by the cells. The PKH26 fluorescence signal observed in microglia was mainly distributed in a punctate pattern within the cytoplasm, which is consistent with the typical distribution reported in the literature following exosome uptake [26, 27]. By utilizing the "EVCount per Cell—remove cropped cells" pipeline for our analysis, we discovered that each cell harbored a higher number of PKH26-labeled second-trimester AF-Exos spots compared to third-trimester AF-Exos, suggesting that second-trimester AF-Exos are internalized more readily (Figure 3C). Nevertheless, this difference did not achieve statistical significance ($p > 0.05$).

These observations may be influenced by two factors: (1) potential differences in cellular uptake of AF-Exos from different gestational stages, and (2) variations in PKH26 labeling efficiency due to lipid composition differences. While we standardized samples by protein concentration, we did not directly assess PKH26 labeling efficiency across gestational stages. Consequently, we cannot definitively distinguish between these possibilities, and the lack of a stringent negative control further limits our interpretation. Nevertheless, our results suggest differential interactions between AF-Exos from different gestational stages and microglia, potentially reflecting distinct neuroinflammatory regulatory functions.

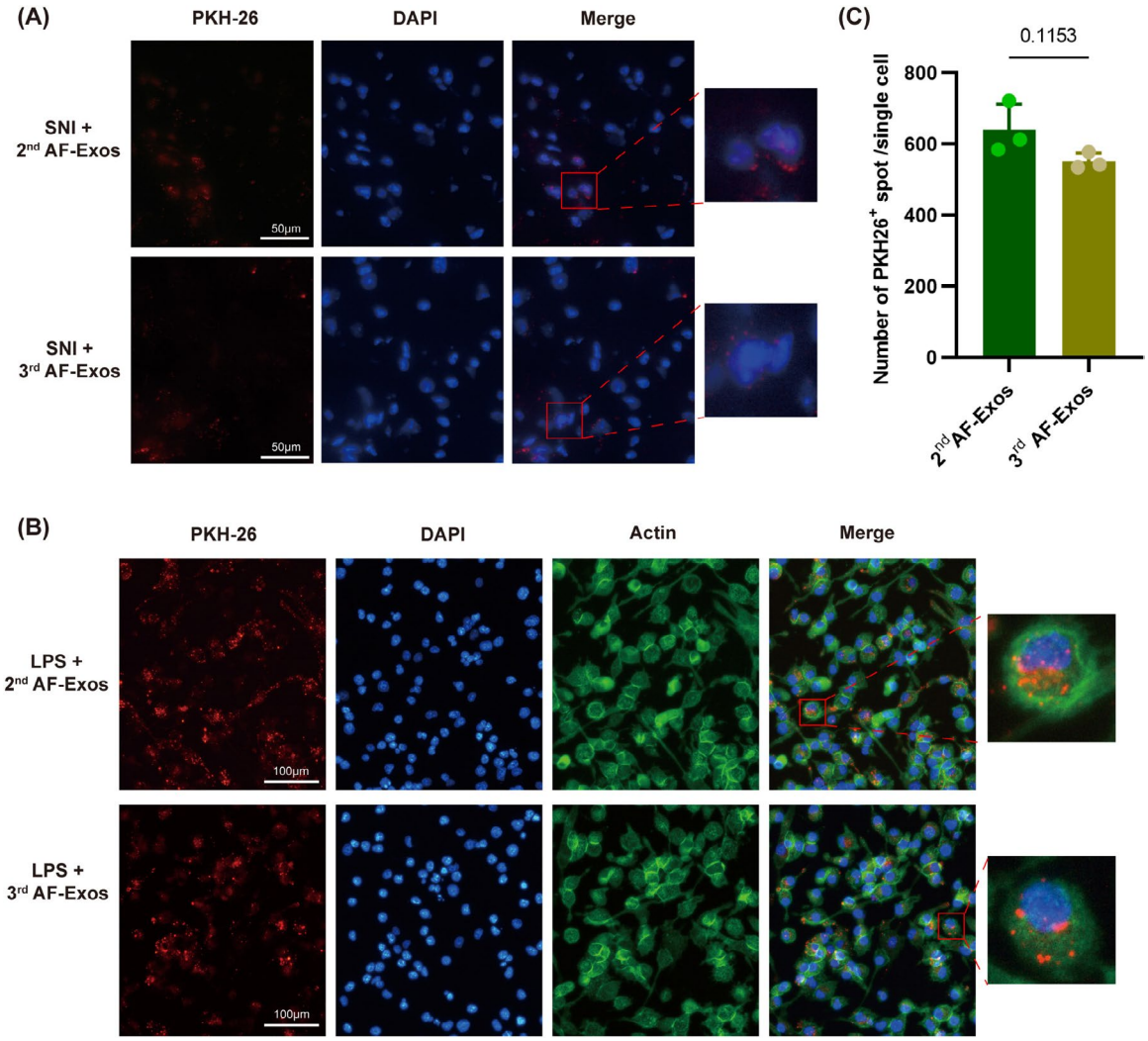

FIGURE 3 | Uptake of human AF-Exos. (A) Representative fluorescent images of AF-Exos (PKH26-labeled, red), nucleus (DAPI, blue), and merged images in the ipsilateral dorsal horn of SNI mice ($n = 3$, scale bar = 50 μm). (B) Representative fluorescent images of AF-Exos (PKH26-labeled, red), nucleus (DAPI, blue), cytoskeleton (Actin, green), and merged images in the LPS-induced BV2 cells ($n = 3$, scale bar = 100 μm). (C) Quantification of PKH26-labeled AF-Exos per single cell in LPS-induced BV2 cells ($n = 3$). Data are presented as mean ± SD and analyzed using an unpaired two-tailed *t*-test; $p > 0.05$.

3.3 | AF-Exos Alleviated Neuropathic Pain and Suppressed Neuroinflammation in SNI Mice

SNI mice that received PBS treatment showed a significantly decreased ipsilateral PWMT compared to the sham mice on Days 3, 5, and 7 after surgery (**$p < 0.01$, ***$p < 0.001$; Figure 4A). Compared with PBS treatment, consecutive intrathecal administration of AF-Exos for 3 days after surgery showed an analgesic effect on Day 3 for SNI-induced mechanical nociceptive sensitization, which persisted until Day 5 ($^{\#}p < 0.05$, $^{\#\#}p < 0.01$, $^{\#\#\#}p < 0.001$). The analgesic efficacy of the second-trimester AF-Exos was superior to that of the third-trimester AF-Exos (Day 5, $^{\wedge}p < 0.05$).

Western blot analysis revealed that SNI significantly increased the expression of IL-1β ($p < 0.01$; Figure 4B), whereas the expression of IL-10 remained unchanged ($p > 0.05$; Figure 4C). Further, AF-Exos treatment significantly attenuated the SNI-induced IL-1β overexpression ($p < 0.01$; Figure 4B) and upregulated IL-10 expression ($p < 0.05$; Figure 4C) in the ipsilateral lumbar spinal cord of SNI mice on Day 7 after surgery.

3.4 | AF-Exos Inhibited Cell Viability and LPS-Induced Neuroinflammation in BV2 Cells

After 24 h of LPS treatment, the cell viability of BV2 cells was significantly reduced ($p < 0.0001$; Figure 5A), likely due to the potent cytotoxic effects of LPS. Moreover, incubation with AF-Exos further decreased the cell viability of LPS-induced BV2 cells ($p < 0.0001$), with second-trimester AF-Exos demonstrating a more pronounced effect ($p < 0.0001$). It is important to note that CCK8 assays specifically measure changes in cellular metabolic activity; therefore, a comprehensive assessment of AF-Exos therapeutic efficacy should incorporate additional parameters, including NO level and inflammatory cytokine profiles.

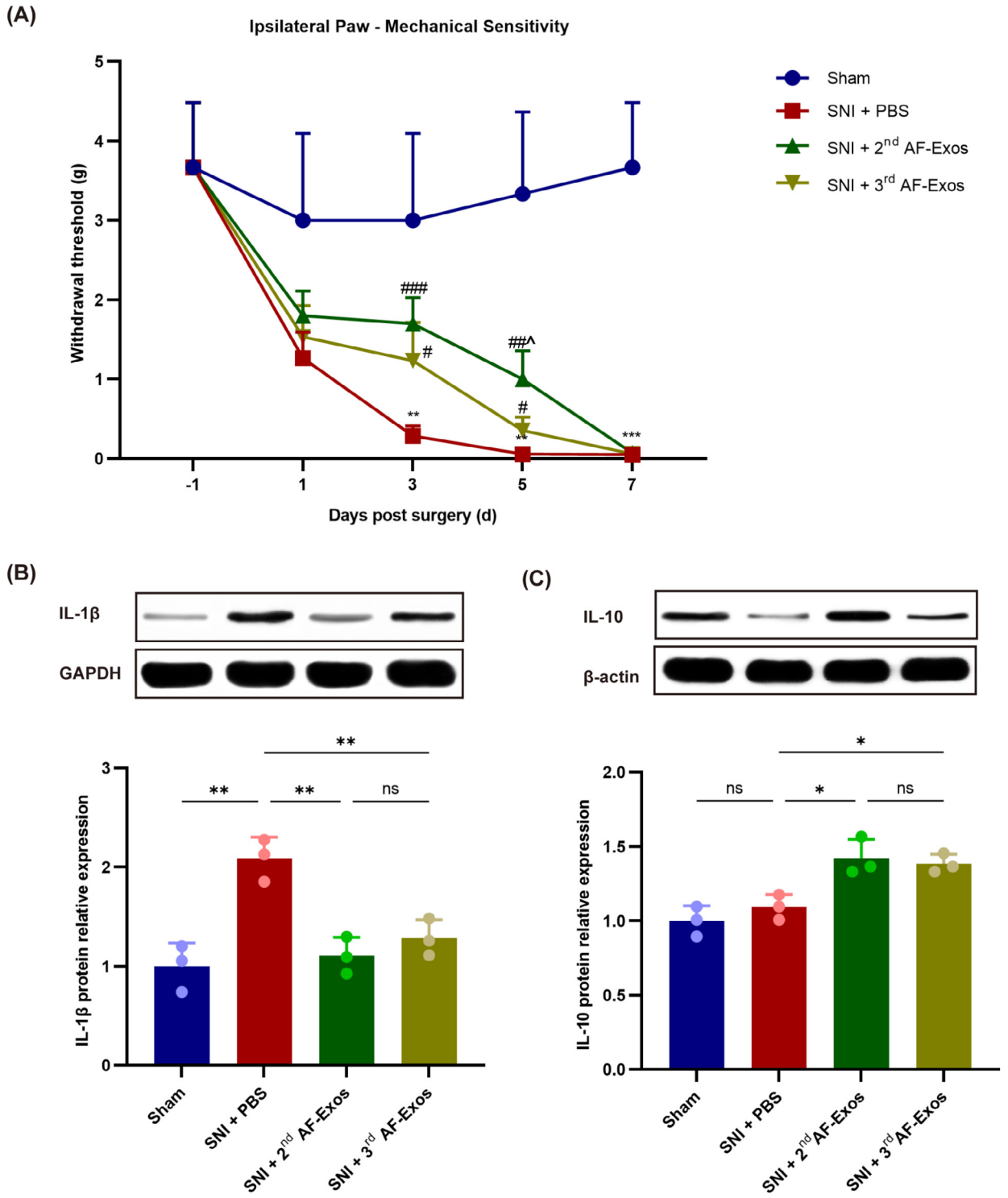

FIGURE 4 | Human AF-Exos alleviated neuropathic pain and suppressed neuroinflammation in SNI mice. (A) Paw withdrawal mechanical threshold (PWMT) was measured using a von Frey filament at indicated time points ($n = 6$). Data are presented as mean ± SD and analyzed using a two-way ANOVA with Bonferroni correction; $^{**}p < 0.01$, $^{***}p < 0.001$, compared with the Sham group; $^{\#}p < 0.05$, $^{\#\#}p < 0.01$, $^{\#\#\#}p < 0.001$, compared with the SNI + PBS group; $^{\wedge}p < 0.05$, compared with the SNI + 3rd AF-Exos group. Representative western blot of (B) IL-1β and (C) IL-10, along with the corresponding statistical analysis ($n = 3$). Data on protein expression are presented as mean ± SD and analyzed using a one-way ANOVA with Bonferroni correction; $^{*}p < 0.05$, $^{**}p < 0.01$.

The NO level ($p < 0.0001$; Figure 5B), mRNA levels of IL-1β ($p < 0.0001$; Figure 5C) and IL-6 ($p < 0.0001$; Figure 5D), and protein level of IL-1β ($p < 0.0001$; Figure 5E) were significantly upregulated in LPS-induced BV2 cells, whereas the mRNA and protein levels of IL-10 did not change significantly ($p > 0.05$; Figure 5F,G). Following AF-Exos intervention, the NO level (LPS + 2nd AF-Exos group, $p < 0.0001$; LPS + 3rd AF-Exos group, $p < 0.01$; Figure 5B), mRNA levels of IL-1β ($p < 0.0001$; Figure 5C) and IL-6 ($p < 0.0001$; Figure 5D), and protein level of IL-1β (LPS + 2nd AF-Exos group, $p < 0.0001$;

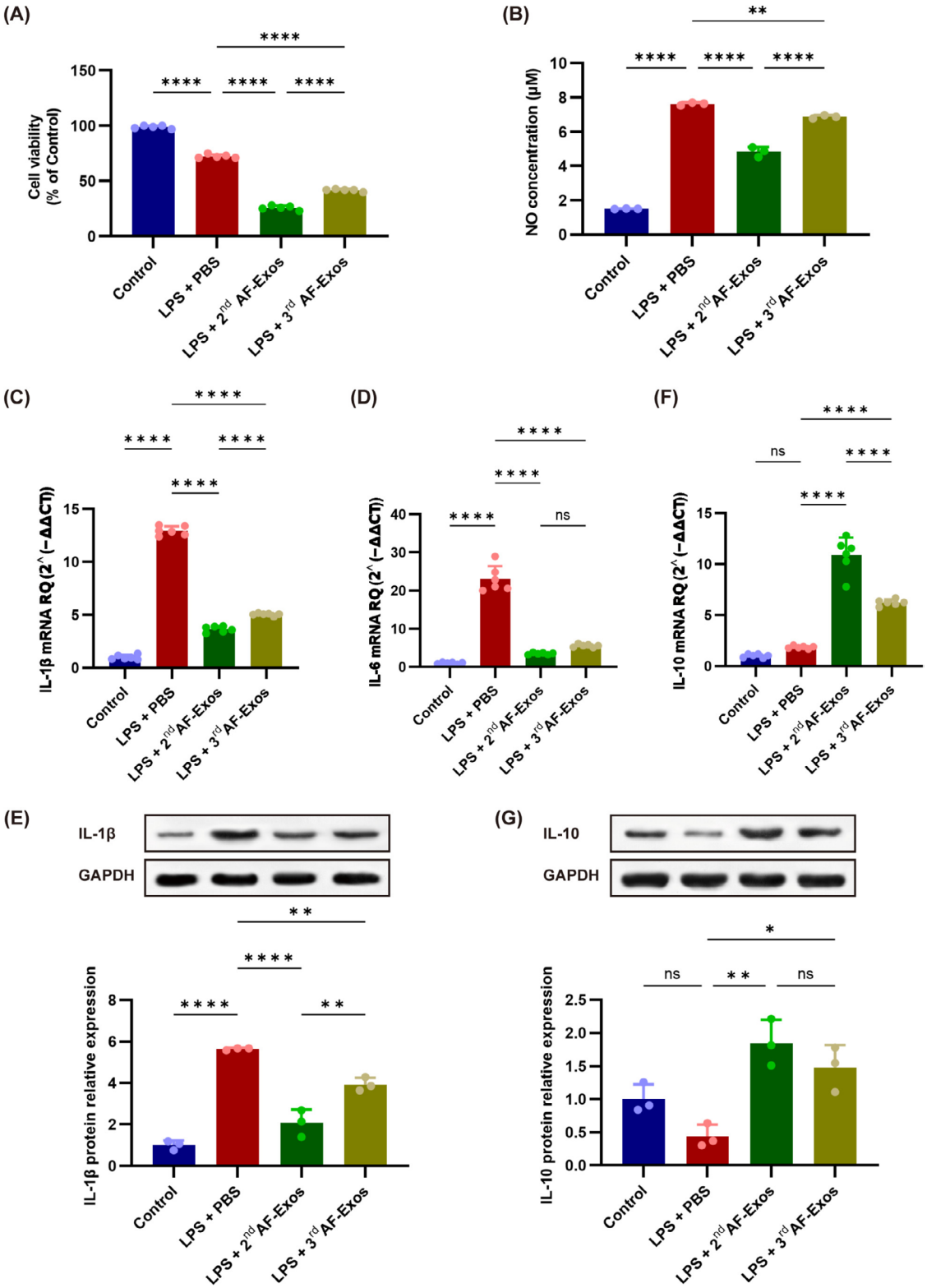

FIGURE 5 | Human AF-Exos inhibited LPS-induced neuroinflammation in BV2 cells. Data of (A) cell viability ($n = 6$) and (B) NO levels ($n = 3$) are presented as mean ± SD and analyzed using a one-way ANOVA with Bonferroni correction; $^{**}p < 0.01$, $^{****}p < 0.0001$. Data on mRNA expression of (C) IL-1β, (D) IL-6, and (F) IL-10 ($n = 6$) are presented as mean ± SD and analyzed using a one-way ANOVA with Bonferroni correction; $^{****}p < 0.0001$. Representative western blot of (E) IL-1β and (G) IL-10, along with the corresponding statistical analysis ($n = 3$). Data on protein expression are presented as mean ± SD and analyzed using a one-way ANOVA with Bonferroni correction; $^{*}p < 0.05$, $^{**}p < 0.01$, $^{****}p < 0.0001$.

LPS + 3rd AF-Exos group, $p < 0.01$; Figure 5E) were decreased, whereas the mRNA ($p < 0.0001$; Figure 5F) and protein (LPS + 2nd AF-Exos group; $p < 0.01$; LPS + 3rd AF-Exos group; $p < 0.05$; Figure 5G) levels of IL-10 were significantly increased. Further, the NO level ($p < 0.0001$; Figure 5B) and mRNA ($p < 0.0001$; Figure 5C) and protein ($p < 0.01$;

Figure 5E) levels of IL-1β were more significantly suppressed in the second-trimester AF-Exos than they were in the third-trimester AF-Exos. Additionally, the mRNA level of IL-10 ($p < 0.0001$; Figure 5F) was more significantly increased in the second-trimester AF-Exos.

3.5 | AF-Exos Promoted Microglia Transition to an Anti-Inflammatory Phenotype in LPS-Induced BV2 Cells

Microglia can modulate neuroinflammation and play a pivotal role in neuropathic pain. Therefore, we investigated whether AF-Exos could affect microglial phenotypic alteration by assessing cellular markers associated with microglial homeostasis. $CD86^+/CD16^+$ microglia are characterized by pro-inflammatory responses, whereas $CD206^+/Arg\text{-}1^+$ microglia exhibit anti-inflammatory phenotypic characteristics and regulatory functions [28, 29]. Flow cytometric analysis revealed an increased ratio of $CD86^+$ to $CD206^+$ cells in LPS-induced BV2 cells ($p < 0.0001$; Figure 6A), which was subsequently attenuated by AF-Exos ($p < 0.0001$).

For further validation, western blot and immunofluorescence were performed to detect CD16 and Arg-1 expression. Western blot results indicated that CD16 expression was upregulated following LPS treatment ($p < 0.001$; Figure 6B), and AF-Exos did not reverse this upregulation. In contrast, Arg-1 expression was downregulated following LPS treatment ($p < 0.0001$), and AF-Exos attenuated this downregulation (LPS + 2nd AF-Exos group, $p < 0.0001$; LPS + 3rd AF-Exos group, $p < 0.05$; Figure 6C), indicating its ability to promote microglial transition to an $Arg\text{-}1^+$

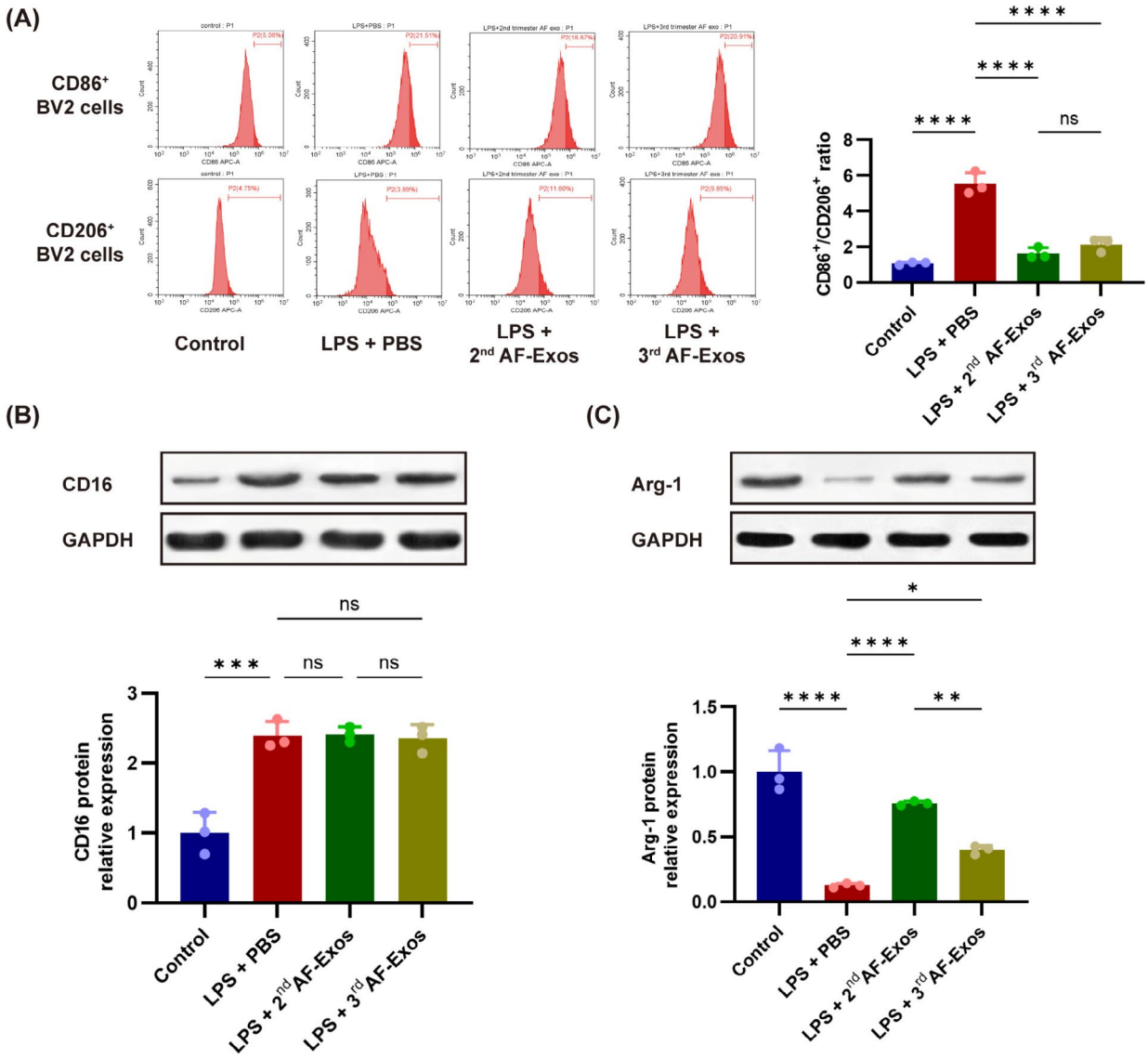

FIGURE 6 | Human AF-Exos modulate LPS-induced microglial phenotype in BV2 cells (flow cytometry and western blot). (A) Flow cytometry results for $CD86^+$ and $CD206^+$ BV2 cells, along with the corresponding statistical analysis of the $CD86^+/CD206^+$ ratio ($n = 3$). Data are presented as mean ± SD and analyzed using a one-way ANOVA with Bonferroni correction; $^{****}p < 0.0001$. Representative western blot of (B) CD16 and (C) Arg-1, along with the corresponding statistical analysis ($n = 3$). Data on protein expression are presented as mean ± SD and analyzed using a one-way ANOVA with Bonferroni correction; $^{*}p < 0.05$, $^{**}p < 0.01$, $^{***}p < 0.001$, $^{****}p < 0.0001$.

phenotype. Notably, the effects of second-trimester AF-Exos were more pronounced than those of third-trimester AF-Exos ($p < 0.01$; Figure 6C).

BV2 cells were examined by immunofluorescence microscopy to visualize the expression and localization of CD16, Arg-1, and CD11b within the cells (Figure 7A,B). The upregulation of CD16 ($p < 0.0001$; Figure 7C) and downregulation of Arg-1 ($p < 0.001$; Figure 7D) following LPS treatment were consistent with the findings of the western blot analysis. Treatment with second-trimester AF-Exos following LPS treatment significantly attenuated CD16 expression ($p < 0.0001$) and partially restored Arg-1 levels ($p < 0.01$). Third-trimester AF-Exos exhibited similar but less pronounced immunomodulatory effects. CD11b expression showed no significant differences among the groups ($p > 0.05$). These findings demonstrate that the $CD86^+/CD16^+$ phenotype is enhanced and the $CD206^+/Arg\text{-}1^+$ phenotype is suppressed in response to LPS stimulation. Moreover, AF-Exos remarkably attenuate neuroinflammation and alleviate neuropathic pain, primarily by promoting microglial transition to the $CD206^+/Arg\text{-}1^+$ phenotype.

4 | Discussion

We observed the pathological changes induced in the spinal cord and the pain-related behavioral alterations on the side of the injury in SNI mice, due to its side-specificity [30, 31]. The internalization of AF-Exos by the ipsilateral dorsal horn and LPS-induced BV2 microglia demonstrates their homing capability, which is consistent with previous research. Specifically, intrathecal exosomes have been shown to exhibit a targeted homing ability to the ipsilateral

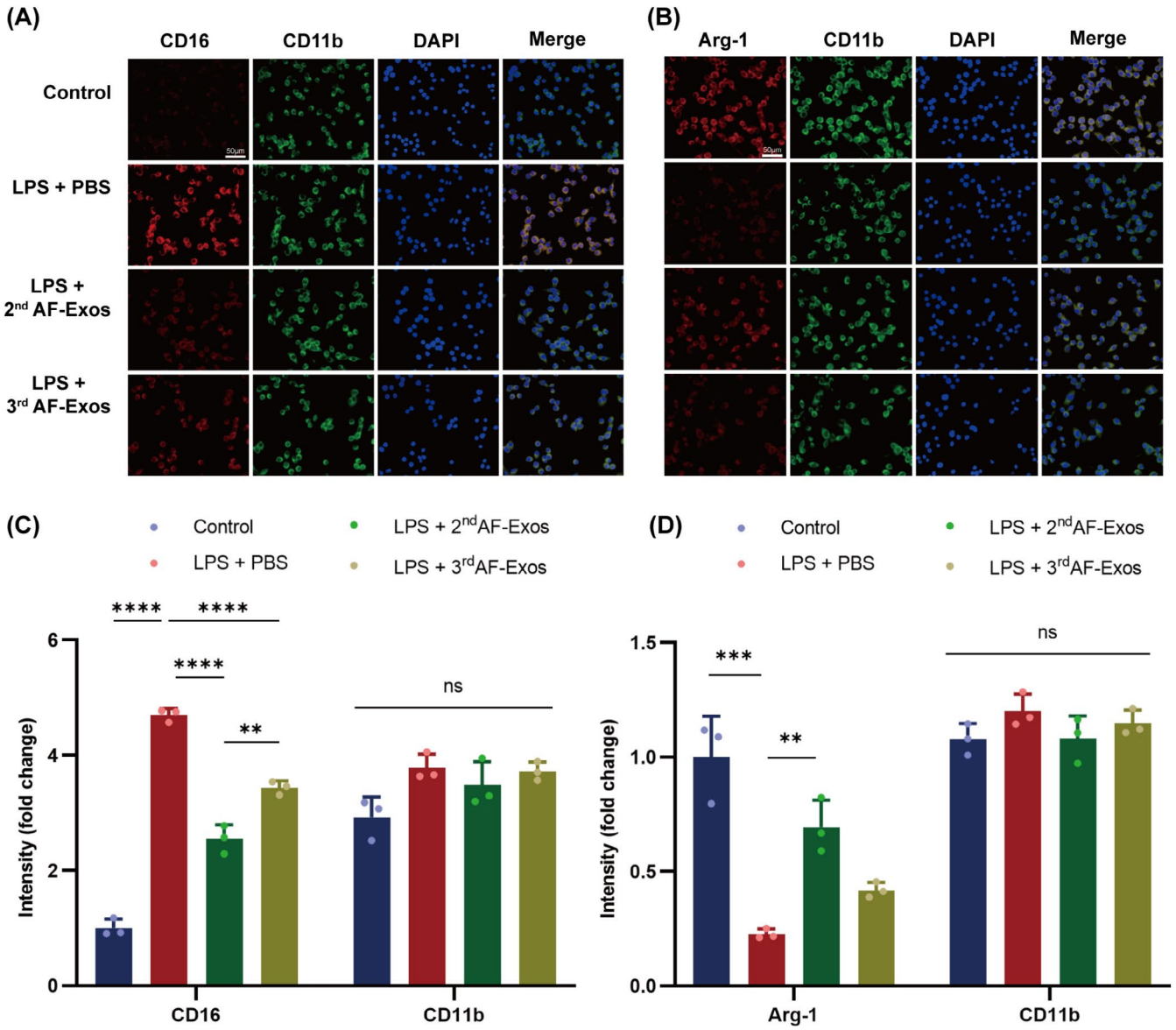

FIGURE 7 | Human AF-Exos modulate LPS-induced microglial phenotype in BV2 cells (immunofluorescence). (A) Representative fluorescent images of CD16 (red), CD11b (green), nucleus (DAPI, blue), and merged images in BV2 cells ($n = 3$, scale bar = 50 μm). (B) Representative fluorescent images of Arg-1 (red), CD11b (green), nucleus (DAPI, blue), and merged images in BV2 cells ($n = 3$, scale bar = 50 μm). Quantification of fluorescence intensity for (C) CD16 and CD11b, as well as (D) Arg-1 and CD11b in BV2 cells ($n = 3$). Data are presented as mean ± SD and analyzed using a one-way ANOVA with Bonferroni correction; $^{**}p < 0.01$, $^{***}p < 0.001$, $^{****}p < 0.0001$.

spinal cord dorsal horn and dorsal root ganglia [32], underscoring their promising potential for precision therapeutic interventions in spinal cord pathological conditions. The homing capability is crucial for the functionality of exosomes, as it ensures that the therapeutic cargo delivered by exosomes—such as proteins, lipids, or nucleic acids—reaches the appropriate sites where it can exert its effects on gene expression and cellular behavior [33–35]. The homing capability of exosomes, combined with the pathological environment such as inflammatory conditions or hypoxia [36, 37], promotes their localization to the area of injury.

While our study did not perform co-localization analysis of exosomes with neuronal markers, which represents a methodological limitation, several studies have provided compelling evidence supporting the therapeutic potential of intrathecally administered exosomes in managing inflammatory and neuropathic pain conditions [38–40]. Notably, Sun et al. [41] successfully demonstrated the precise distribution of exosomes within the spinal dorsal horn following intrathecal injection, further substantiating the translational significance of our research. Intrathecal administration of AF-Exos for three consecutive days after surgery showed a significant analgesic effect in SNI mice, which persisted until Day 5 after surgery, indicating long-lasting analgesic effects of AF-Exos on neuropathic pain.

Microglial-mediated neuroinflammation is an important pathological process associated with neuropathic pain [28]. Neuroinflammation occurs with the release of pro-inflammatory mediators like NO, IL-1β, and IL-6. In addition, anti-inflammatory mediators, such as IL-10, are released during neuroinflammation, which may be part of a complex mechanism that prevents an excessive response [42]. In this study, AF-Exos exhibited a suppressive effect on the expression of IL-1β and promoted the expression of IL-10 in SNI mice. In in vitro experiments, we found that AF-Exos can suppress the metabolic state of BV2 cells, thereby indirectly reducing inflammatory levels, which is consistent with the effects observed with EVs derived from amniotic fluid stem cells (AFSCs) and other anti-neuroinflammatory agents [21, 43]. Additionally, AF-Exos reversed the alterations in pro-inflammatory (NO, IL-1β, IL-6) and anti-inflammatory (IL-10) factors in BV2 cells, which may attenuate the triggered inflammatory cascade and promote nerve repair [44]. Therefore, AF-Exos may achieve analgesia by balancing the expression of pro- and anti-inflammatory factors.

IL-1β and IL-6 are classic pro-inflammatory factors involved in enhanced pain perception and the induction of neuroinflammation and neuropathic pain [45]. Excessive and sustained release of IL-1β and IL-6 promotes the recruitment of inflammatory cells. This, in turn, triggers the release of prostaglandin E2 and NO, stimulating both local and systemic inflammatory responses [46, 47]. IL-10 exhibits an immunosuppressive function, thereby attenuating the tissue injury caused by an excessive and uncontrolled inflammatory response and inducing pain anti-hypersensitivity in neuropathic pain models [48, 49]. It also participates in neural injury prevention and maintains neuronal homeostasis by regulating synaptic function [50]. The modulation of neuroinflammation by AF-Exos is potentially mediated through the regulation of microglial homeostasis. Promoting microglia to transition to an anti-inflammatory profile can alleviate neuropathic pain by decreasing neuroinflammation [51, 52]. In this study, AF-Exos significantly promoted the transition of microglia towards a phenotype expressing CD206 and Arg-1 cell markers. This phenotypic transition modulates the balance between pro-inflammatory and anti-inflammatory effects, directly suppressing neuroinflammation in the dorsal horn of the injured spinal cord and consequently facilitating neuroprotection and analgesic effects.

Human AF-Exos obtained during the second trimester exhibited superior anti-inflammatory effects compared to those obtained during the third trimester, both in vivo and in vitro. The varying cargo of AF-Exos from different trimesters could be a contributing factor. Human amniotic fluid exhibits heterogeneity, with different components present in the same pregnant woman across different gestational trimesters, indicating distinct paracrine potential [21]. The level of IL-10 in amniotic fluid, which induces transition to the anti-inflammatory phenotype of microglia, is negatively correlated with gestational age [28, 53]. Furthermore, exosomes containing heat shock protein 72, which can suppress immune activity, have been identified in second-trimester amniotic fluid [54]. Moreover, in a mouse model, exosomes abundant in pro-inflammatory factors increased as the gestational age progressed [55], thereby triggering the release of inflammatory factors by microglia [28]. Omics analysis reveals that second-trimester exosomes exhibit superior anti-inflammatory properties, while third-trimester exosomes prioritize metabolic and endothelial maintenance. These differences primarily stem from variations in HSPD1/PAI-1 pathway activation and the differential enrichment of key miRNAs like miR-21-5p [12]. These factors may contribute to the better analgesic efficacy of AF-Exos derived from the second trimester, attributable to their significantly stronger anti-inflammatory capabilities.

Exosomes generally exhibit lower immunogenicity and can effectively prevent immune rejection reactions [56, 57]. Notably, exosomes derived from human amniotic fluid have been investigated as a cell-free, less immunogenic, and non-toxic therapeutic approach in mouse models of acute liver failure, with no observable immune responses [58]. Furthermore, EVs derived from human AFSCs have been shown to reduce T cell proliferation, contributing to the attenuation of potential immune responses [21]. This property indirectly confirms their characteristic low immunogenicity. In our study, we closely monitored the mice for any signs of adverse reactions following repeated intrathecal administration of human AF-Exos. We did not observe any overt immune-related side effects such as behavioral abnormalities, weight loss, or other signs of distress that would indicate significant immunological rejection. Hence, the utilization of human-derived exosomes in animal models not only enhances our understanding of the biological mechanisms underlying human diseases but also provides novel insights for developing therapeutic strategies [59].

Although numerous studies have focused on the immunosuppressive effect of AFSC exosomes [23, 60], prolonged in vitro expansion can alter the epigenetic landscape of donor cells (e.g.,

DNA methylation and histone modification), which in turn affects the molecular composition of their EVs. Culture variables such as seeding density and passage number markedly influence EV yield, bioactivity, and molecular profiles. Continuous passaging of cells leads to epigenetic drift, resulting in altered cargo and diminished regenerative potential [61–63]. AF Exos constitute a minimally manipulated, developmentally enriched vesicle population with simple and feasible acquisition, independent of cellular proliferation, function, or senescence, whose native neuroimmune cargo offers distinct advantages for neuropathic pain modulation.

Human AF-Exos possess the capacity to directly target the neuroimmune axis, thereby offering promising opportunities for the development of scalable therapeutic options; hence, they can be used as biologically derived therapeutic agents. However, our study had certain limitations, including the absence of a comprehensive analysis of exosome composition, which could have provided valuable insights into their role in modulating microglial homeostasis. Additionally, we did not investigate the signaling pathways that mediate the conversion of microglia to an anti-inflammatory phenotype. Another limitation is that our study focused on ipsilateral data, resulting in a deficient understanding of the systemic effects of human AF-Exos. In the future, we plan to conduct a compositional analysis of AF-Exos and examine both ipsilateral and contralateral data to clarify the underlying mechanisms by which AF-Exos modulate the phenotypic transition in microglia during neuropathic pain.

In conclusion, our study demonstrated that treatment with AF-Exos promoted the transition of microglia to an anti-inflammatory phenotype and inhibited neuroinflammation, resulting in the alleviation of neuropathic pain in SNI mice. These findings highlight the substantial therapeutic potential of AF-Exos for the treatment of neuropathic pain.

Author Contributions

Yong Yang, Qulian Guo, and Ping Li conceived and designed the research. Qian Li, Hang Dai, Sha Zhang, Lin Peng, and Yulu Chen performed the methodology, formal analysis, and investigation. Qian Li, and Hang Dai prepared the original draft, while Qian Li, and Yong Yang reviewed and edited the manuscript. Yong Yang acquired funding, and Qulian Guo, and Yong Yang provided resources and supervision. All authors read and approved the final manuscript.

Acknowledgments

This work was supported by the Natural Science Foundation of Hunan Province (grant number 2022JJ30975). The authors acknowledge Editage (www.editage.com) for professional English language editing. During the preparation of this work, the authors used OpenAI's ChatGPT-4.0 in order for language refinement. After using this tool/service, the authors reviewed and edited the content as needed and took full responsibility for the content of the publication.

Disclosure

The authors have nothing to report.

Conflicts of Interest

The authors declare no conflicts of interest.

Data Availability Statement

The data that support the findings of this study are available in the Methods and/or Results of this article.

References

1. B. H. Smith, H. L. Hébert, and A. Veluchamy, "Neuropathic Pain in the Community: Prevalence, Impact, and Risk Factors," *Pain* 161, no. Suppl 1 (2020): S127–S137, https://doi.org/10.1097/j.pain.0000000000001824.

2. K. Bannister, J. Sachau, R. Baron, and A. H. Dickenson, "Neuropathic Pain: Mechanism-Based Therapeutics," *Annual Review of Pharmacology and Toxicology* 60 (2020): 257–274, https://doi.org/10.1146/annurev-pharmtox-010818-021524.

3. N. B. Finnerup, R. Kuner, and T. S. Jensen, "Neuropathic Pain: From Mechanisms to Treatment," *Physiological Reviews* 101, no. 1 (2021): 259–301, https://doi.org/10.1152/physrev.00045.2019.

4. N. T. Fiore, S. R. Debs, J. P. Hayes, S. S. Duffy, and G. Moalem-Taylor, "Pain-Resolving Immune Mechanisms in Neuropathic Pain," *Nature Reviews. Neurology* 19, no. 4 (2023): 199–220, https://doi.org/10.1038/s41582-023-00777-3.

5. M.-D. Zhang, J. Kupari, J. Su, et al., "Neural Ensembles That Encode Nocifensive Mechanical and Heat Pain in Mouse Spinal Cord," *Nature Neuroscience* 28 (2025): 1012–1023, https://doi.org/10.1038/s41593-025-01921-6.

6. V. Staikopoulos, S. Qiao, J. Liu, et al., "Graded Peripheral Nerve Injury Creates Mechanical Allodynia Proportional to the Progression and Severity of Microglial Activity Within the Spinal Cord of Male Mice," *Brain, Behavior, and Immunity* 91 (2021): 568–577, https://doi.org/10.1016/j.bbi.2020.11.018.

7. B.-C. Jiang, T.-Y. Ding, C.-Y. Guo, et al., "NFAT1 Orchestrates Spinal Microglial Transcription and Promotes Microglial Proliferation via c-MYC Contributing to Nerve Injury-Induced Neuropathic Pain," *Advanced Science* 9, no. 27 (2022): e2201300, https://doi.org/10.1002/advs.202201300.

8. R. C. Paolicelli, A. Sierra, B. Stevens, et al., "Microglia States and Nomenclature: A Field at Its Crossroads," *Neuron* 110, no. 21 (2022): 3458–3483, https://doi.org/10.1016/j.neuron.2022.10.020.

9. L.-W. Zhang, C.-A. Cui, C. Liu, et al., "Auraptene-Ameliorating Depressive-Like Behaviors Induced by Lipopolysaccharide Combined With Chronic Unpredictable Mild Stress in Mice Mitigate Hippocampal Neuroinflammation Mediated by Microglia," *International Immunopharmacology* 136 (2024): 112330, https://doi.org/10.1016/j.intimp.2024.112330.

10. A. Mirarchi, E. Albi, and C. Arcuri, "Microglia Signatures: A Cause or Consequence of Microglia-Related Brain Disorders?," *International Journal of Molecular Sciences* 25, no. 20 (2024): 10951, https://doi.org/10.3390/ijms252010951.

11. X. Xu, H. Chen, Y. Qiu, et al., "Intravenous Application of Human Umbilical Cord Mesenchymal Stem Cells Alleviate Neuropathic Pain by Suppressing Microglia Activation in Rats," *Heliyon* 10, no. 12 (2024): e32689, https://doi.org/10.1016/j.heliyon.2024.e32689.

12. A. Costa, D. Ceresa, A. De Palma, et al., "Comprehensive Profiling of Secretome Formulations From Fetal- and Perinatal Human Amniotic Fluid Stem Cells," *International Journal of Molecular Sciences* 22, no. 7 (2021): 3713, https://doi.org/10.3390/ijms22073713.

13. Y. Ren, F. Wang, R. Sun, et al., "The Genetic Selection of HSPD1 and HSPE1 Reduce Inflammation of Liver and Spleen While Restraining the Growth and Development of Skeletal Muscle in Wuzhishan Pigs," *Animals (Basel)* 14, no. 1 (2024): 174, https://doi.org/10.3390/ani14010174.

14. V. De Paolis, F. Maiullari, M. Chirivì, et al., "Unusual Association of NF-κB Components in Tumor-Associated Macrophages (TAMs)

Promotes HSPG2-Mediated Immune-Escaping Mechanism in Breast Cancer," *International Journal of Molecular Sciences* 23, no. 14 (2022): 7902, https://doi.org/10.3390/ijms23147902.

15. M. Omatsu, Y. Nakanishi, K. Iwane, et al., "THBS1-Producing Tumor-Infiltrating Monocyte-Like Cells Contribute to Immunosuppression and Metastasis in Colorectal Cancer," *Nature Communications* 14, no. 1 (2023): 5534, https://doi.org/10.1038/s41467-023-41095-y.

16. G. Bhatti, R. Romero, N. Gomez-Lopez, et al., "The Amniotic Fluid Proteome Changes With Gestational Age in Normal Pregnancy: A Cross-Sectional Study," *Scientific Reports* 12, no. 1 (2022): 601, https://doi.org/10.1038/s41598-021-04050-9.

17. C. M. Bowen, F. S. Ditmars, A. Gupta, J.-A. Reems, and W. S. Fagg, "Cell-Free Amniotic Fluid and Regenerative Medicine: Current Applications and Future Opportunities," *Biomedicine* 10, no. 11 (2022): 2960, https://doi.org/10.3390/biomedicines10112960.

18. T. Del Rivero, J. Milberg, C. Bennett, M. I. Mitrani, and M. A. Bellio, "Human Amniotic Fluid Derived Extracellular Vesicles Attenuate T Cell Immune Response," *Frontiers in Immunology* 13 (2022): 977809, https://doi.org/10.3389/fimmu.2022.977809.

19. M. Ghafourian, R. Mahdavi, Z. Akbari Jonoush, et al., "The Implications of Exosomes in Pregnancy: Emerging as New Diagnostic Markers and Therapeutics Targets," *Cell Communication and Signaling: CCS* 20, no. 1 (2022): 51, https://doi.org/10.1186/s12964-022-00853-z.

20. K. Bai, X. Li, J. Zhong, et al., "Placenta-Derived Exosomes as a Modulator in Maternal Immune Tolerance During Pregnancy," *Frontiers in Immunology* 12 (2021): 671093, https://doi.org/10.3389/fimmu.2021.671093.

21. A. Costa, R. Quarto, and S. Bollini, "Small Extracellular Vesicles From Human Amniotic Fluid Samples as Promising Theranostics," *International Journal of Molecular Sciences* 23, no. 2 (2022): 590, https://doi.org/10.3390/ijms23020590.

22. M. Schürz, J. Danmayr, M. Jaritsch, et al., "EVAnalyzer: High Content Imaging for Rigorous Characterisation of Single Extracellular Vesicles Using Standard Laboratory Equipment and a New Open-Source ImageJ/Fiji Plugin," *Journal of Extracellular Vesicles* 11, no. 12 (2022): e12282, https://doi.org/10.1002/jev2.12282.

23. H. Katifelis, E. Filidou, A. Psaraki, et al., "Amniotic Fluid-Derived Mesenchymal Stem/Stromal Cell-Derived Secretome and Exosomes Improve Inflammation in Human Intestinal Subepithelial Myofibroblasts," *Biomedicine* 10, no. 10 (2022): 2357, https://doi.org/10.3390/biomedicines10102357.

24. J. Kowal, G. Arras, M. Colombo, et al., "Proteomic Comparison Defines Novel Markers to Characterize Heterogeneous Populations of Extracellular Vesicle Subtypes," *Proceedings of the National Academy of Sciences of the United States of America* 113, no. 8 (2016): E968–E977, https://doi.org/10.1073/pnas.1521230113.

25. R. Samaeekia, B. Rabiee, I. Putra, et al., "Effect of Human Corneal Mesenchymal Stromal Cell-Derived Exosomes on Corneal Epithelial Wound Healing," *Investigative Ophthalmology & Visual Science* 59, no. 12 (2018): 5194–5200, https://doi.org/10.1167/iovs.18-24803.

26. L. Yan, Y. Cao, L. Hou, et al., "Ginger Exosome-Like Nanoparticle-Derived miRNA Therapeutics: A Strategic Inhibitor of Intestinal Inflammation," *Journal of Advanced Research* 69 (2025): 1–15, https://doi.org/10.1016/j.jare.2024.04.001.

27. C. Park, Z. Lei, Y. Li, et al., "Extracellular Vesicles in Sepsis Plasma Mediate Neuronal Inflammation in the Brain Through miRNAs and Innate Immune Signaling," *Journal of Neuroinflammation* 21, no. 1 (2024): 252, https://doi.org/10.1186/s12974-024-03250-0.

28. A. A. Atta, W. W. Ibrahim, A. F. Mohamed, and N. F. Abdelkader, "Microglia Polarization in Nociplastic Pain: Mechanisms and Perspectives," *Inflammopharmacology* 31, no. 3 (2023): 1053–1067, https://doi.org/10.1007/s10787-023-01216-x.

29. L.-Q. Zhang, S.-J. Gao, J. Sun, et al., "DKK3 Ameliorates Neuropathic Pain via Inhibiting ASK-1/JNK/p-38-Mediated Microglia Polarization and Neuroinflammation," *Journal of Neuroinflammation* 19, no. 1 (2022): 129, https://doi.org/10.1186/s12974-022-02495-x.

30. I. Decosterd and C. J. Woolf, "Spared Nerve Injury: An Animal Model of Persistent Peripheral Neuropathic Pain," *Pain* 87, no. 2 (2000): 149–158, https://doi.org/10.1016/S0304-3959(00)00276-1.

31. F. Guida, D. De Gregorio, E. Palazzo, et al., "Behavioral, Biochemical and Electrophysiological Changes in Spared Nerve Injury Model of Neuropathic Pain," *International Journal of Molecular Sciences* 21, no. 9 (2020): 3396, https://doi.org/10.3390/ijms21093396.

32. S.-J. Shiue, R.-H. Rau, H.-S. Shiue, et al., "Mesenchymal Stem Cell Exosomes as a Cell-Free Therapy for Nerve Injury-Induced Pain in Rats," *Pain* 160, no. 1 (2019): 210–223, https://doi.org/10.1097/j.pain.0000000000001395.

33. Y. Liang, Z. Iqbal, J. Lu, et al., "Cell-Derived Nanovesicle-Mediated Drug Delivery to the Brain: Principles and Strategies for Vesicle Engineering," *Molecular Therapy* 31, no. 5 (2023): 1207–1224, https://doi.org/10.1016/j.ymthe.2022.10.008.

34. N. L. Syn, L. Wang, E. K. Chow, C. T. Lim, and B. C. Goh, "Exosomes in Cancer Nanomedicine and Immunotherapy: Prospects and Challenges," *Trends in Biotechnology* 35, no. 7 (2017): 665–676, https://doi.org/10.1016/j.tibtech.2017.03.004.

35. H. Wei, Q. Chen, L. Lin, et al., "Regulation of Exosome Production and Cargo Sorting," *International Journal of Biological Sciences* 17, no. 1 (2021): 163–177, https://doi.org/10.7150/ijbs.53671.

36. F. J. Verweij, L. Balaj, C. M. Boulanger, et al., "The Power of Imaging to Understand Extracellular Vesicle Biology In Vivo," *Nature Methods* 18, no. 9 (2021): 1013–1026, https://doi.org/10.1038/s41592-021-01206-3.

37. D. J. Schneider, J. M. Speth, L. R. Penke, S. H. Wettlaufer, J. A. Swanson, and M. Peters-Golden, "Mechanisms and Modulation of Microvesicle Uptake in a Model of Alveolar Cell Communication," *Journal of Biological Chemistry* 292, no. 51 (2017): 20897–20910, https://doi.org/10.1074/jbc.M117.792416.

38. T. Hua, M. Yang, H. Song, et al., "Huc-MSCs-Derived Exosomes Attenuate Inflammatory Pain by Regulating Microglia Pyroptosis and Autophagy via the miR-146a-5p/TRAF6 Axis," *Journal of Nanobiotechnology* 20 (2022): 324, https://doi.org/10.1186/s12951-022-01522-6.

39. Z. Lin, X. Luo, J. R. Wickman, et al., "Inflammatory Pain Resolution by Mouse Serum-Derived Small Extracellular Vesicles," *Brain, Behavior, and Immunity* 123 (2025): 422–441, https://doi.org/10.1016/j.bbi.2024.09.032.

40. M. Akhlaghpasand, R. Tavanaei, M. Hosseinpoor, et al., "Safety and Potential Effects of Intrathecal Injection of Allogeneic Human Umbilical Cord Mesenchymal Stem Cell-Derived Exosomes in Complete Subacute Spinal Cord Injury: A First-In-Human, Single-Arm, Open-Label, Phase I Clinical Trial," *Stem Cell Research & Therapy* 15, no. 1 (2024): 264, https://doi.org/10.1186/s13287-024-03868-0.

41. Q. Sun, R. X. Weng, Y. C. Li, et al., "Potentiation of Visualized Exosomal miR-1306-3p From Primary Sensory Neurons Contributes to Chronic Visceral Pain via Spinal P2X3 Receptors," *Pain* (2025), https://doi.org/10.1097/j.pain.0000000000003537.

42. F. Leng and P. Edison, "Neuroinflammation and Microglial Activation in Alzheimer Disease: Where Do We Go From Here?," *Nature Reviews. Neurology* 17, no. 3 (2021): 157–172, https://doi.org/10.1038/s41582-020-00435-y.

43. J. Zhang, Y. Zheng, Y. Luo, Y. Du, X. Zhang, and J. Fu, "Curcumin Inhibits LPS-Induced Neuroinflammation by Promoting Microglial M2 Polarization via TREM2/ TLR4/ NF-κB Pathways in BV2 Cells," *Molecular Immunology* 116 (2019): 29–37, https://doi.org/10.1016/j.molimm.2019.09.020.

44. C. S. Subhramanyam, C. Wang, Q. Hu, and S. T. Dheen, "Microglia-Mediated Neuroinflammation in Neurodegenerative Diseases," *Seminars in Cell & Developmental Biology* 94 (2019): 112–120, https://doi.org/10.1016/j.semcdb.2019.05.004.

45. R.-R. Ji, Z.-Z. Xu, and Y.-J. Gao, "Emerging Targets in Neuroinflammation-Driven Chronic Pain," *Nature Reviews. Drug Discovery* 13, no. 7 (2014): 533–548, https://doi.org/10.1038/nrd4334.

46. C. Gabay, C. Lamacchia, and G. Palmer, "IL-1 Pathways in Inflammation and Human Diseases," *Nature Reviews Rheumatology* 6, no. 4 (2010): 232–241, https://doi.org/10.1038/nrrheum.2010.4.

47. T. Tanaka, M. Narazaki, and T. Kishimoto, "Interleukin (IL-6) Immunotherapy," *Cold Spring Harbor Perspectives in Biology* 10, no. 8 (2018): a028456, https://doi.org/10.1101/cshperspect.a028456.

48. W. Ouyang and A. O'Garra, "IL-10 Family Cytokines IL-10 and IL-22: From Basic Science to Clinical Translation," *Immunity* 50, no. 4 (2019): 871–891, https://doi.org/10.1016/j.immuni.2019.03.020.

49. M.-Y. Deng, K. A. Ahmad, Q.-Q. Han, et al., "Thalidomide Alleviates Neuropathic Pain Through Microglial IL-10/β-Endorphin Signaling Pathway," *Biochemical Pharmacology* 192 (2021): 114727, https://doi.org/10.1016/j.bcp.2021.114727.

50. K. Ren and R. Torres, "Role of Interleukin-1beta During Pain and Inflammation," *Brain Research Reviews* 60, no. 1 (2009): 57–64, https://doi.org/10.1016/j.brainresrev.2008.12.020.

51. H. Yang, L. Wu, H. Deng, et al., "Anti-Inflammatory Protein TSG-6 Secreted by Bone Marrow Mesenchymal Stem Cells Attenuates Neuropathic Pain by Inhibiting the TLR2/MyD88/NF-κB Signaling Pathway in Spinal Microglia," *Journal of Neuroinflammation* 17, no. 1 (2020): 154, https://doi.org/10.1186/s12974-020-1731-x.

52. N. T. Fiore, J. P. Hayes, S. I. Williams, and G. Moalem-Taylor, "Interleukin-35 Alleviates Neuropathic Pain and Induces an Anti-Inflammatory Shift in Spinal Microglia in Nerve-Injured Male Mice," *Brain, Behavior, and Immunity* 122 (2024): 287–300, https://doi.org/10.1016/j.bbi.2024.07.043.

53. J. Apuzzio, Y. Chan, A. Al-Khan, N. Illsley, P.-L. Kim, and S. Vonhaggen, "Second-Trimester Amniotic Fluid Interleukin-10 Concentration Predicts Preterm Delivery," *Journal of Maternal-Fetal & Neonatal Medicine* 15, no. 5 (2004): 313–317.

54. S. S. Witkin, I. M. Linhares, A. M. Bongiovanni, C. Herway, and D. Skupski, "Unique Alterations in Infection-Induced Immune Activation During Pregnancy," *BJOG: An International Journal of Obstetrics and Gynaecology* 118, no. 2 (2011): 145–153, https://doi.org/10.1111/j.1471-0528.2010.02773.x.

55. S. Sheller-Miller, J. Trivedi, S. M. Yellon, and R. Menon, "Exosomes Cause Preterm Birth in Mice: Evidence for Paracrine Signaling in Pregnancy," *Scientific Reports* 9, no. 1 (2019): 608, https://doi.org/10.1038/s41598-018-37002-x.

56. L. Zhu, H. T. Sun, S. Wang, et al., "Isolation and Characterization of Exosomes for Cancer Research," *Journal of Hematology & Oncology* 13, no. 1 (2020): 152, https://doi.org/10.1186/s13045-020-00987-y.

57. C. Zhou, B. Zhang, Y. Yang, et al., "Stem Cell-Derived Exosomes: Emerging Therapeutic Opportunities for Wound Healing," *Stem Cell Research & Therapy* 14, no. 1 (2023): 107, https://doi.org/10.1186/s13287-023-03345-0.

58. A. Psaraki, D. Zagoura, L. Ntari, et al., "MFGE-8 Identified in Fetal Mesenchymal-Stromal-Cell-Derived Exosomes Ameliorates Acute Hepatic Failure Pathology," *iScience* 26, no. 11 (2023): 108100, https://doi.org/10.1016/j.isci.2023.108100.

59. M. Cieślik, K. Nazimek, and K. Bryniarski, "Extracellular Vesicles-Oral Therapeutics of the Future," *International Journal of Molecular Sciences* 23, no. 14 (2022): 7554, https://doi.org/10.3390/ijms23147554.

60. A. Cargnoni, A. Papait, A. Masserdotti, et al., "Extracellular Vesicles From Perinatal Cells for Anti-Inflammatory Therapy," *Frontiers in Bioengineering and Biotechnology* 9 (2021): 637737, https://doi.org/10.3389/fbioe.2021.637737.

61. A. Rai, B. Claridge, J. Lozano, and D. W. Greening, "The Discovery of Extracellular Vesicles and Their Emergence as a Next-Generation Therapy," *Circulation Research* 135, no. 1 (2024): 198–221, https://doi.org/10.1161/circresaha.123.323054.

62. J. Liu, Y. Ding, Z. Liu, and X. Liang, "Senescence in Mesenchymal Stem Cells: Functional Alterations, Molecular Mechanisms, and Rejuvenation Strategies," *Frontiers in Cell and Development Biology* 8 (2020): 258, https://doi.org/10.3389/fcell.2020.00258.

63. M. de Almeida Fuzeta, N. Bernardes, F. D. Oliveira, et al., "Scalable Production of Human Mesenchymal Stromal Cell-Derived Extracellular Vesicles Under Serum-/Xeno-Free Conditions in a Microcarrier-Based Bioreactor Culture System," *Frontiers in Cell and Developmental Biology* 8 (2020): 553444, https://doi.org/10.3389/fcell.2020.553444.